Solar cooking potential in Switzerland: nodal modelling and optimization

Timothée Chatelain[a], Dasaraden Mauree[a,*], Samson Taylor[a], Olivia Bouvard[a], Jérémy Fleury[a], Luc Burnier[a], Andreas Schüler[a]

[a] *Solar Energy and Building Physics Laboratory, Ecole Polytechnique Fédérale de Lausanne, Lausanne, Switzerland*

Abstract

Solar cooking is one possible solution to reduce the domination of fossil fuel in the domestic sector and to benefit from renewable energy. This study assesses the solar cooking potential in Switzerland. A nodal model, based on energy balance equations of a box-type solar cooker is implemented in Matlab. Model parameters that cannot be determined experimentally or analytically are evaluated through an optimization procedure based on a Genetic Algorithm (GA). The model is able to predict the temperature of the cooking vessel with an average relative error around 5%. Based on its reliability, the model is simulated over a year for different locations in Switzerland in order to determine the solar cooking potential. It is characterized by a metric that represents the number of days in a year the oven could be used to cook potatoes for two persons. It is found that the cooking times of potatoes can be well predicted by an Arrhenius law with an activation energy of 74.14 $\left[\frac{\mathrm{kJ}}{\mathrm{mol}}\right]$. The potato cooking criterion is based on the Arrhenius equation and determines if the pot simulated temperature profile of a particular day allows to cook potatoes. The North-East of Switzerland is the least favourable area for solar cooking with theoretically around 155 cooking days per year. Around 240 days are estimated to be suitable for cooking in the cantons of Valais and Grisons, which represents a significant potential for solar cooking in Switzerland.

Keywords: Solar cooker, Nodal modelling, Genetic algorithm, Arrhenius law, Potatoes cooking

Highlights

- New method using nodal models developed for evaluating the performance of a box-type solar cooker.
- Genetic algorithms used to estimate model parameters that cannot be determined experimentally.
- Metric designed to estimate the cooking days potential at the national scale of Switzerland.
- Reproducible method means it can be generalized everywhere.

1. Introduction

Solar energy is abundant on the Earth's surface but, its low density and the important mass contained in the atmosphere do not allow to naturally reach temperatures high enough to cook food. An early description of a solar cooker or solar oven appears in the work of the

*Corresponding author
Email address: dasaraden.mauree@gmail.com (Dasaraden Mauree)

Swiss Physicist Horace de Saussure in 1767 (Saxena et al., 2011). He built what he called an "Héliothermomètre", a wood box with cork insulation and three glass layers (de Saussure, 1784). Nowadays, due to the increasing pressure on fossil energy sources, there is a renewed interest in solar energy exploitation and solar cookers (Schwarzer and da Silva, 2008; Geddam et al., 2015; Yettou et al., 2014; Esen, 2004). The first known prototype of the kind dates from the early 1950s in India (Panwar et al., 2012). In the following years, several designs and mounting configurations have been tested and their performances assessed. Enhancement of the efficiency has been achieved by adding sun tracking system (Al-Soud et al., 2010). Nowadays, solar ovens are still built as an insulated box with transparent glass cover but in addition they integrate, most of the time, reflective surfaces (booster mirrors) to increase the performance Yettou et al. (2014). The energy is absorbed through the black paint of the inner wall or redirected to an absorber plate at the bottom through a reflecting inner wall. Box-type solar ovens are typically used to cook food around at $100°C$.

Various parameters exist to measure the performance of box-type solar cookers (Saxena et al., 2011). They are determined mostly by measuring the temperatures, time and solar irradiation under controlled conditions. While these parameters are useful to compare solar cooker designs to each other, they do not give an indication of their potential along the year for a specific the location. For this reason, a model was developed to determine a new metric providing information on the number of days per year when the solar cooker can be used for each location using meteorological database.

Most of the work done on solar cookers is through experimentation while modelling aspects that would allow a yearly simulation at a national scale have not been well developed. Solar ovens are modelled by separating the oven into several components and assigning a uniform temperature for each component. Heat balance equations are then discretized and solved for the temperatures for each time step. Terres et al. (2014) and Guidara et al. (2017) identified five and six components, respectively, with solar irradiation and ambient temperature as inputs to the models. Maximum relative errors with the measured temperature inside the oven inferior to 4% are reached. It is possible to estimate several parameters of the model by minimizing the difference between the measured and the simulated temperature inside the solar oven (Saxena et al., 2011). This procedure is used by Soria-Verdugo (2015) to find the optimal values of the convective heat transfer coefficients which are relatively difficult to estimate otherwise. The very large majority of experiments in the literature are performed in African or South European countries. The reason for this is the abundant solar irradiation and relatively high ambient temperature in these regions and thus a high potential for solar cooking. Currently, solar cooking technology is not very popular in Switzerland. With around 1000 $\left[\frac{\mathrm{kWh}}{\mathrm{m}^2}\right]$ per year of solar irradiation, Switzerland is indeed less propitious for the development of this technology. However, this amount of solar energy is already sufficient to cook food during some days of the year although the full potential has not yet been assessed. Switzerland offers many isolated areas especially in the mountains where fuel supply for cooking not easy and where solar oven utilization could be judicious. One way of assessing this potential would be to actually try the oven at different locations and determine its performance with a number of criteria. This is however laborious and time consuming. Another more convenient way is to use a mathematical model of the oven which could simulate its behaviour under different conditions and assess its performance.

The objective of the present study is to develop a nodal model of the solar oven ULOG manufactured by the SOLEMYO organisation (Association Solemyo, 2019) (a Swiss organisation that develops solar ovens with natural and raw materials: wood box, wool insulation). The ULOG is a simple isolated wooden box with an inclined two-layers glazing. The model must be able to reproduce and predict the inside oven temperature with solar irradiation and ambient temperature inputs. Experiments are done to determine the thermal and physical properties

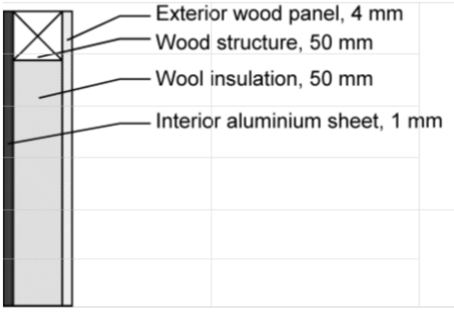

Figure 1: Oven wall

of the oven. When theories are available, the experimentally determined values are compared with the result of theoretical correlations. Other tests are performed by placing the oven under solar exposure and by monitoring temperatures of different cooker components in order to obtain reference data for the model validation. An optimization algorithm is used to determine some parameters of the oven that are difficult to evaluate theoretically. A new metric is also developed to assess the performance of the ULOG by characterizing the oven and quantifying its possible utilization. This metric represents the number of days during a year when the solar oven can be used to cook food in a given region. The solar oven is simulated for a typical year with solar irradiation and ambient temperature of different locations in Switzerland. The metric is then used to geographically analyse the solar cooking potential.

2. Method

2.1. Oven description

The ULOG is a basic solar oven made by SOLEMYO (Association Solemyo, 2019). The walls are constructed with a wooden structure filled with around 5cm of bulk sheep wool (a cheap and raw insulating material) as shown in Fig. 1. The inner walls are covered with a thin aluminium black foil. The glazing has an angle of 30° with the horizontal and has a square area of 0.5m over 0.5m. The double glazing is composed of two 3mm thick clear glasses with an interior air layer of 24mm. The glass layers are inserted in the wooden frame. The base of the ULOG solar oven has a dimension of 66.5 cm x 61 cm. With the reflector closed, it has a maximum height of 45 cm and with the reflector completely open it reaches a maximum height of 95 cm. The weight without recipients or food is 9 kg.

This oven has two positions: one optimized for low sun positions during winter and one more adapted for the solar rays coming from high in the sky. It is possible to position it as shown in Fig. 2 or on the other edge. This study has been done with the oven positioned in summer mode. A reflector of the same size as the glazing can also be added to increase the solar gains in the oven. It is fixed at the top of the glazing in the wooden frame with two hinges.

2.2. Nodal model

The basis of a nodal analysis is to subdivide a complex system into several elemental units, or nodes, which represent a physical component of the initial structure like a surface or a volume (Olsommer et al., 1997). It is then assumed that the physical properties, the temperature and the heat flux of a node are uniform. The nodes exchange heat through convection, conduction or radiation modes. The nodes are connected in a network where each connection is described by a thermal resistance that characterizes the heat transfer between the nodes.

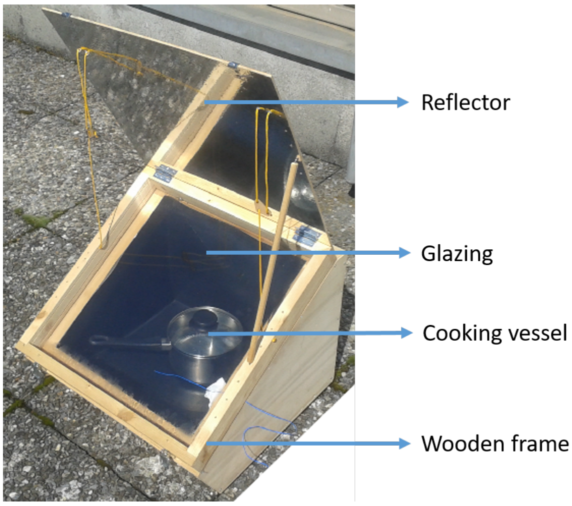

Figure 2: ULOG oven from SOLEMYO

Each of the nodes has two physical properties: a temperature T and a capacitance C (Associates, 2000). The capacitance is defined as the product between the mass m_i and the specific heat capacity c_{pi} of the corresponding node i :

$$C_i = m_i c_{pi}. \tag{1}$$

The thermal resistance R_{ij} characterizes the heat exchange between the nodes i and j. It is also common to refer to the conductance G_{ij}, defined as the inverse of the thermal resistance :

$$G_{ij} = \frac{1}{R_{ij}} \quad \text{with} \quad G_{ij} = G_{ji}. \tag{2}$$

The governing equations of the nodal model are the heat balance equations applied for each node. The heat transfers from all the connecting nodes j must be taken into account. For node i, it is written as :

$$C_i \frac{dT_i}{dt} = \sum_j G_{ij}(T_j - T_i). \tag{3}$$

The time derivative of the temperature is discretized with Euler schemes. To avoid problems with the stability of the solution, an implicit Euler method is preferred :

$$C_i \frac{T_i^{n+1} - T_i^n}{\Delta t} = \sum_j G_{ij}(T_j^{n+1} - T_i^{n+1}). \tag{4}$$

By fixing the initial conditions T_i^0, Equation 4 can be solved to determine the temperature at each time step.

The solar oven ULOG is divided into the seven following nodes:

- Node 1: Cooking vessel
- Node 2: All surfaces corresponding to the inner wall
- Node 3: All surfaces corresponding to the outer wall

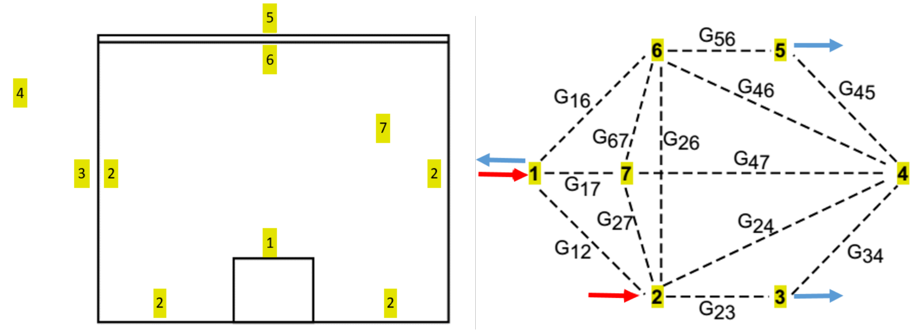

Figure 3: Schematic representation of the ULOG oven and the corresponding nodal network, conductances, energy inputs (red arrows) and energy loss (blue arrows)

Table 1: ULOG oven dimensions. The subscript number corresponds to the identified numbers as referred to in Fig.3.

	A_1	A_2	A_3	A_5	A_6
Surface area, $[m^2]$	0.1767	0.4	0.7	0.2025	0.2025

- Node 4: Ambient air
- Node 5: Outer glass pane
- Node 6: Inner glass pane
- Node 7: Inside air

They are schematically represented in Fig. 3 with the conductances characterizing the heat transfer between the nodes.

The surface area of the other components can be found in Table 1. The red arrows represent the energy inputs of the system. These inputs are modelled as solar gains G through the glass layers. A fixed fraction of the solar gains, depending on the solar oven geometry, is absorbed by the inner wall and the rest by the cooking vessel. A value of 20% has been calculated for this solar cooker, based on experimental data collected at the laboratory.

2.3. *Experimental measurements*

This study is based upon experiments conducted at the Solar Energy and Building Physics Laboratory (LESO-PB) and includes work on the optical and thermal properties of the ULOG's glazing and measurement of the oven air leakage. The following section details the experimental measures that have been conducted.

2.3.1. *Temperature measurements*

In order to validate the nodal model, an experiment is set up on the laboratory roof to measure the temperature inside the oven when exposed to solar irradiation (see Fig. 4). The solar oven with the cooking vessel inside is placed to face the South, away from any shadow.

Figure 4: Experimental setup for temperature measurements under solar irradiation (left) and for determination of the U-value (right)

K-type thermocouples are used to record the temperature inside the oven. One thermocouple is fixed on the back of the cooking vessel, hidden from direct solar irradiation. It corresponds to the temperature T_1 of the pot. The second thermocouple is placed on the bottom of the oven to measure T_2, the temperature of the inner wall. Its location is also chosen in order to not receive direct solar irradiation. The reflector is not installed on the solar oven. This reduces the complexity of the model since the reflector adds modelling parameters such as the angles between the reflector, the oven and the Sun. Temperatures are recorded every 30 seconds. Several measurements were done starting from March 2018, during sunny days but also when there was cloud cover. Experiments usually started around 10am and ended at 5pm. This experiment was performed five times with 1L of water in the cooking vessel, on the 11th, 12th, 19th, 24th and 26th of April 2018.

2.3.2. U-values

The experiments detailed above are performed during transient phenomena, such as the heating up of the oven. But it is also interesting to perform experiments at stationary conditions to evaluate, for instance, the U-value of the oven's walls and window. U is the overall heat transfer coefficient. This coefficient is related to the heat $\dot{Q}$ going through the element with surface area A by the relation 5 :

$$\dot{Q} = AU\Delta T, \tag{5}$$

where ΔT is the difference between the room temperature and the air temperature inside the oven.

Such a test is performed in the laboratory by heating up the air inside the solar oven with two electric resistances that deliver 20 W of heat each (see Fig. 4). Supports are built to hold the resistances vertically in order to heat up the air and not directly the inner surface of the wall. Inside air, inner wall and inner glass temperatures are recorded with the same thermocouples as in the experiments described above. They reach relatively quickly a stationary state when the heat losses balance the heat supply of the heaters. The air temperature inside the oven is measured at two different locations: close to the bottom and to the top of the box. The mean temperature between the two is considered as the inside air temperature. A fluxmeter is then used to measure the heat flux through the different surfaces of the oven. Measurements of the heat flux are made at five different instants to increase the accuracy. The ambient temperature in the laboratory is constant at 22°C.

G_{46} and G_{24} represent the heat losses due to the thermal bridges of the oven. They are difficult to measure but they can be deduced from the U-value experiment. The heat balance at steady-state is written as :

$$\dot{Q}_{heater} \quad = \quad U_{wall}A_{wall}\Delta T \;+\; U_{glass}A_{glass}\Delta T \;+\; \left(\psi_{frame}L_{frame} + \psi_{oven}L_{oven}\right)\Delta T. \quad (6)$$

The heat supplied by the heaters $\dot{Q}_{heater}$ equals the heat losses through the walls, the window and the thermal bridges of the window frame and the oven. ψ_{frame} and ψ_{oven} are the linear thermal transmittances of the thermal bridges and L_{frame} and L_{oven} are the length of the thermal bridges. $\psi_{frame}L_{frame}$ and $\psi_{oven}L_{oven}$ are respectively equal to G_{46} and G_{24} and since the other terms of Equation 31 are known, the thermal bridges can be determined. The thermal losses due to the thermal bridges are equally distributed among G_{24} and G_{46}.

2.3.3. Infiltration rate

The infiltration rate is measured by artificially increasing the concentration of carbon dioxide in the oven and monitoring its decrease over time. Both the infiltration rate and the concentration of carbon dioxide of the room are assumed constant. In that case, the concentration of CO_2 in the oven follows a diffusion equation whose solution corresponds to an exponential decay. By fitting the measurements with a function such as $ae^{-\lambda t}$, the air leakage mass flow $\dot{m}_{leak}$ can be found through the parameter λ which represents the infiltration rate. The air leakage mass flow is simply given by

$$\dot{m}_{leak} = \frac{\lambda \rho_{air} V_{oven}}{3600}, \quad (7)$$

where ρ_{air} is the air density and V_{oven} is the air volume inside the oven. The conductance G_{47} is therefore evaluated as the quantity

$$G_{47} = \dot{m}_{leak} c_{p,air}, \quad (8)$$

with $c_{p,air}$ being the specific heat capacity of air.

2.4. Model parameters

Depending on the physical heat transfer mode they represent, conductances are evaluated in different manners. Conductive conductance is defined as

$$G_{ij} = \frac{kA_i}{L}, \quad (9)$$

where k is the thermal conductivity, A_i the cross-sectional area through which heat flows and L is the length between the two nodes.

For convective heat transfers, the following formula is used

$$G_{ij} = hA_i, \quad (10)$$

where h is the convective heat transfer coefficient and A_i is the area of the node i in contact with the fluid.

The heat transfer coefficient is evaluated through the Nusselt number Nu with the relation

$$Nu = \frac{hL}{k}, \quad (11)$$

where L is a characteristic length and k is the conductivity of the fluid, air in the present case. According to Churchill and Chu (1975), convective heat transfer at the surface of a vertical plate is governed by

$$Nu = \left(0.825 + \frac{0.387 Ra^{1/6}}{\left(1 + \left(\frac{0.492}{Pr}\right)^{9/16}\right)^{8/27}}\right)^2, \quad (12)$$

with the Prandtl number Pr set to 0.7 and the Rayleigh number Ra.

Equation 12 is valid for the exchanges between the lateral surface of the pot and the air inside as well as between the vertical inner and outer oven side walls and the air. The characteristic length of these surfaces is their height. Correlations that take into account the effect of the wind on the heat transfer coefficient are also available and could be used. It is indeed an important element which affects the outside convective heat transfer. Its effect is however neglected in this study.

From Baehr and Stephan (2011), the convective heat transfer at the lid is characterized by the following equations

$$Nu = 0.54 Ra^{1/4}, \text{ if } 10^4 \leq Ra \leq 10^7 \tag{13}$$

$$Nu = 0.15 Ra^{1/3}, \text{ if } 10^7 \leq Ra \leq 10^{11}. \tag{14}$$

The characteristic length is this time the ratio between the area A and the perimeter P of the horizontal surface. The total heat transfer coefficient between the cooking vessel and the inner air, h_{17} is evaluated as a weighted average between the lid and the lateral surfaces contributions, as

$$h_{17} = \frac{A_{cv,v} h_{cv,v} + A_{cv,lid} h_{cv,lid}}{A_{cv}}, \tag{15}$$

with $A_{cv,v}$ and $h_{cv,v}$ representing respectively the surface area and the heat transfer coefficient of the cooking vessel's lateral surface. Similarly $A_{cv,lid}$ and $h_{cv,lid}$ characterize the surface and the heat transfer of the lid. A_{cv} is the total surface area of the cooking vessel.

Equation 12 holds for the inclined glazing with the difference that the gravity g has to be replaced by its component parallel to the inclined glazing. This is given by the quantity $g \sin\left(\frac{\pi}{6}\right)$. From Saha et al. (2007), the inclination and the space between the two layers of the glazing are too high to neglect the convection mode. The Nusselt number characterizing the convection between the two glass layers is given by the following formula from Incropera et al. (2013):

$$Nu = 0.42 Ra^{\frac{1}{4}} Pr^{0.012} \left(\frac{H}{L}\right)^{-0.3}. \tag{16}$$

It is a function of the aspect ratio, the height H and width L of the enclosure.

The formulation for the radiative exchanges is slightly different than the conduction and convection modes. The heat flux $\dot{q}$ is indeed dependent on the temperatures to the power four. In order to have analytical solutions available, the surfaces are assumed to be gray diffuse. It means that the radiative properties of the surface such as emissivity, absorptivity, reflectance are independent of the wavelength and the direction of the irradiation (Modest, 2003). For such surfaces, net radiative heat flux $\dot{q}_i$ from surface i among N surfaces is defined as:

$$\frac{\dot{q}_i}{\epsilon_i} - \sum_{j=1}^{N} \left(\frac{1}{\epsilon_j} - 1\right) F_{ij} \dot{q}_j = E_{b,i} - \sum_{j=1}^{N} F_{ij} E_{b,j}, \; i = 1, .., N. \tag{17}$$

$E_{b,i}$ is the black body emissive power of the surface i, evaluated as $\sigma \epsilon_i T_i^4$. σ is the Boltzmann's constant equal to $5.67 \cdot 10^{-8} \left[\frac{\mathrm{W}}{\mathrm{m^2 K^4}}\right]$ and ϵ_i is the emissivity of the node i. F_{ij} is the view factor between nodes i and j and only depends on the geometry. When $N = 2$, one equation for each $\dot{q}_i$ is derived from Equation 17. This may be solved for $\dot{q}_1$ by eliminating $\dot{q}_2$

$$\dot{q}_1 = \frac{\epsilon_1 \sigma \left(T_1^4 - F_{12} T_2^4\right) + \epsilon_1 (1 - \epsilon_2) \sigma F_{12} \left(T_2^4 - F_{21} T_1^4\right)}{1 - (1 - \epsilon_1)(1 - \epsilon_2) F_{12} F_{21}}. \tag{18}$$

Table 2: K_i coefficients

K_0	K_2	K_4	K_6	K_8
0.8214	-2.17e-5	8.05e-9	-3.28e-12	5.36e-29

Once the view factors are determined, radiative heat fluxes can be calculated with Equation 18.

For simple geometries such as two parallel flat plates, the view factors are equal to 1 and Equation 18 reduces to a simple form

$$\dot{Q}_{ij} = G_{ij}(T_j^4 - T_i^4), \tag{19}$$

with the conductance given by

$$G_{ij} = \frac{A_i \sigma}{\frac{1}{\epsilon_i} + \frac{1}{\epsilon_j} - 1}. \tag{20}$$

Equation 20 is valid for the radiative exchange between the two glass layers.

According to Mannan (2005), most monatomic and diatomic gases are non-participating media. Moreover, the relatively small air volume confined in the oven limits the interactions between the radiation and the air. The inside air is thus considered as a non-participating medium. Therefore, it has no influence on the radiative heat exchanges.

The nodes' capacitance are other parameters needed by the model. The cooking vessel is made of iron. The specific heat capacity of iron is taken from the literature and a balance is used to know the mass. The capacitance of the water is taken into account in a similar way. Due to the heterogeneous structure of the oven walls, it is not straightforward to determine their capacitances. The walls are made of a thin aluminium foil on the inner side, a wood structure filled with wool and a thin wood panel at the exterior. The mass of every component is estimated for a particular wall. Their masses are then multiplied by their specific heat capacity and the sum of these results corresponds to the capacitance of the particular wall. The same procedure is applied for each wall and the sum represents the global wall capacitance of the oven.

The solar gains G enter the system through the glass layers. The solar radiation absorbed by the exterior wooden wall of the oven is neglected. Solar gains are characterized by the solar heat gain coefficient g, or g-value, defined as the ratio between the radiative flux going through a transparent construction element and the total incident radiative flux (Gnansounou, 2014).

g is usually divided in a value for direct irradiation g_{dir} and a value for the diffuse irradiation g_{diff}. The coefficient for the direct irradiation is a function of the incident angle γ of the solar beams while g_{diff} is defined as the value of g_{dir} at 60° of incidence.

The Zenith angle of the Sun is assumed to be such that the solar beams are always perpendicular to the glass window. Its position in the plan perpendicular to the glazing is then determined by the incident angle γ. g_{dir} is written as a polynomial function of γ:

$$g_{dir} = K_0 + K_2\gamma^2 + K_4\gamma^4 + K_6\gamma^6 + K_8\gamma^8. \tag{21}$$

The reference $\gamma = 0°$ is determined in the normal direction of the glass window. Experiments have been previously conducted in the LESO-PB to evaluate K_i and the results are presented in the Table 2.

The solar irradiation is divided into a direct component i_{dir} and a diffuse component i_{diff}. The irradiation coming from reflection from the ground is treated with an albedo coefficient A_{bd} of 0.2. Solar gains are therefore the sum of three components: the direct irradiation, the diffuse

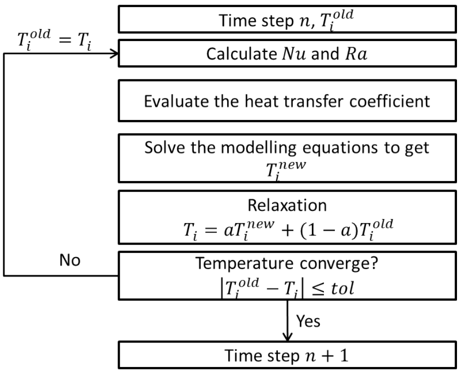

Figure 5: Resolution algorithm

irradiation from the atmosphere and the surroundings and the reflected irradiation from the ground. The solar gains are thus evaluated as:

$$G = g_{dir} i_{dir} \left(A^*_{glass} + A^*_{refl}\right) + g_{diff} i_{diff} A_{glass} \left(\frac{5}{6} + \frac{1}{6} A_{bd}\right), \quad (22)$$

where A^*_{glass} and A_{glass} are respectively the apparent and the real surface area of the glass window, with $A^*_{glass} = \cos\left(\frac{\gamma\pi}{180}\right) A_{glass}$. A^*_{refl} is the apparent area of the reflectors, if any. The factors $\frac{5}{6}$ and $\frac{1}{6}$ take into account the fact that the window is not horizontal but has an angle of 30° with the horizontal.

i_{dir} and i_{diff} data are available from the LESO-PB meteorological station. The meteorological station of the laboratory monitors also the ambient temperature T_4 and it is thus available as input to the model.

The angles defining the Sun's position, the Zenith and the Azimuth, are taken from the calculator (Solar Topo, 2019). They are evaluated at the point with latitude 46.51°N and longitude 6.63°E which corresponds to the city of Lausanne.

In order to have a rough estimation of the effects of the reflector on the solar cooking potential, it is included in the model simulation in a simplified way. In a similar way to Sethi et al. (2014), an optimal angle of the ULOG reflector can be determined in function of the Sun's Zenith angle. It would however imply to continuously adapt the reflector angle, which considerably increases the complexity of the model. To avoid this problematic, the reflector is assumed to be fixed and aligned with the vertical. Following the method presented by Sethi et al. (2014), this position is optimal for a Sun elevation of around 30°. The reflector contribution is evaluated at this optimal Sun angle. In that case the apparent surface of the reflector A^*_{refl} is equal to $A_{glass} \cos\left(\frac{\pi}{6}\right)$, knowing the glazing and the reflector have the same surface area.

The solving method is summarized in Fig. 5.

2.5. Optimization

Optimization is performed on the important parameters in order to fit the model output to the measurements since some of the parameters cannot be determined experimentally. Genetic Algorithm (GA) is used as an optimization method (Banos et al., 2011).

Single objective optimization is conducted. The objective function to minimize uses the least squares method, which is the square of the difference between the measured and the simulated cooking vessel temperature, $T_{1,mes}$ and T_1 respectively. In order to increase the validity of the optimization, data of all the available measurements are given to the objective function. This yields the following expression:

$$\text{Obj} = \sum_{n} \underbrace{\left(T_1^n - T_{1,Mes}^n\right)^2}_{\text{Measurement 1}} + \underbrace{\left(T_1^n - T_{1,Mes}^n\right)^2}_{\text{Measurement 2}} + \underbrace{\left(T_1^n - T_{1,Mes}^n\right)^2}_{\text{Measurement 3}} + ..., \quad (23)$$

where the index n refers to the time step.

To assess the robustness of the optimization procedure, the same problem is optimized with AMPL (A Mathematical Programming Language), a modelling language to describe and solve large-scale optimization, among other mathematical problems (Fourer et al., 2003). The MINOS solver is used for the optimization procedure.

Five set of temperature measurements are available and are given to the objective function. Upper and lower bounds are set on the important parameters determined by the sensitivity analysis. The bounds are fixed as plus and minus 30% of their nominal values to give flexibility to the optimization and take into account the uncertainties on the calculated parameters values. The only constraint is that the capacitances of the two glass layers C_5 and C_6 must be equal, since the two layers are supposed to be identical. To take into account the evaporation process of water taking place at the constant temperature of 100°C, the temperature increase in the model is limited.

2.6. Potato cooking

Potato cooking experiments have been made at four different temperatures: 70, 80, 90 and 100°C. The cooking times t_c are evaluated for each cooking temperatures. The water is first heated up to the set point temperature. Five medium potatoes are then immersed and this instant corresponds to the beginning of the cooking time calculation. Even though objective methods such as the evaluation of the Young's modulus depression (Blahovec et al., 2000) have been developed to determine potato cooking, the simple test of the force required to insert a pointed knife in the potatoes is used to evaluate the doneness of the potatoes and the corresponding cooking time t_c.

2.6.1. Potato days metric

This metric corresponds to the number of days during a year where the solar oven could be used to cook food in Switzerland. A day is a "potato day", when it is possible to cook five medium potatoes in 1 L of water, corresponding to food for two persons. Two criteria must be satisfied for such a day: a threshold temperature, under which it is assumed the potatoes would never cook, must be reached and during a sufficient time to transfer enough energy to the potatoes. Löf (1963) showed that the energy required for physical and chemical cooking processes is small compared to the energy needed to increase food temperature and balance heat losses. Thus, knowing the evolution of the water temperature is the only requirement to define if the potatoes are cooked.

The cooking process of the potatoes is assumed to follow an Arrhenius type behaviour:

$$r = Be^{-\frac{\phi}{RT}}. \quad (24)$$

The exponential term depends on the activation energy ϕ of the reaction, the universal gas constant R and the temperature T. The constant B is a characteristic of the chemical reaction. It is common to use this theory in lifetime estimation of items under specific constraints (Schüler et al., 2000) and in cooking processes (Petrou et al., 2002) which both involve chemical processes. In the first case, the rate constant r is replaced by the lifetime and by the cooking time t_c in the second case. With potatoes, the main reaction is the “cooking” of the starch, or gelatinization, whose activation energy must be determined. Equation 24 is thus rewritten as:

$$t_c = Be^{-\frac{\phi}{RT}}. \tag{25}$$

It must be noted that in a $\frac{1}{T}$ against $\ln t_c$ plot, Equation 25 becomes a straight line whose slope is equal to the ratio $-\frac{\phi}{R}$. The cooking times evaluated for four different cooking temperatures are plotted. Then the slope of the interpolated straight line of these four points give the activation energy of the potatoes cooking process, with R fixed at $8.314\left[\frac{\mathrm{J}}{\mathrm{molK}}\right]$. Once the cooking times are determined, the constant B can be determined by Equation 25. It is assumed that this constant characterizes the cooking chemical reactions and thus is similar for all potato cooking experiments. Its final value is set as the average of the four results for the four experiments.

To ensure the potatoes are ready, a cooking criterion CC is defined as:

$$CC = \int_0^{t_c} B\, e^{-\frac{\phi}{RT}}\, dt. \tag{26}$$

This quantity is similar for the four cooking tests, with variations less than 5%, and is a good indicator of the doneness of the potato. Thus for a day to be cookable, it must fulfill the following requirement:

$$\int_{t_0}^{t_{end}} B\, e^{-\frac{\phi}{RT}}\, dt \geq CC, \tag{27}$$

with t_0 and t_{end} being respectively the starting time and ending time of the cooking period. Equation 27 is integrated numerically in Matlab with the temperature profile of T_1 evaluated with the model.

The model is simulated over a year with solar and ambient data for different locations in Switzerland and the ”potato days” are evaluated for each Swiss location following the procedure described previously. The software Meteonorm (Remund, 2008; Remund et al., 2010) gives access to a year of data for 70 meteorological stations in Switzerland. Data are interpolated in Matlab in order to have a time step of 30 seconds on which the model is based. To reduce the computing time, the solar oven is simulated only from 9:30am to 18:00pm each day. The results are analysed with a Geographic Information System software, QGIS, in order to represent them on a map of the Swiss territory.

2.7. Conventional thermal performance parameters

Performance ratings are a useful tool for the comparison of oven types. The most commonly used includes the figure of merits F_1 and F_2 developed by Mullick et al. (1987) and the cooking power P as defined by Funk (2000). F_1 is determined without water load in the cooking vessel and based on the maximal stagnation temperature the oven reaches. It characterizes the no-load conditions and is determined using Eq. 28.

$$F_1 = \frac{T_{ps} - T_{as}}{H_s}, \tag{28}$$

where T_{ps} is maximum absorber plate temperature, T_{as} is ambient air temperature (at stagnation) and H_s is the insolation on a horizontal surface at the stagnation time (in W m^{-2}).

$F_2$and P_s are obtained from measurements when the solar oven is loaded with water. F_2 is calculated using Eq. 29.

$$F'\eta_0 C_R = F_2 = \frac{F_1 (MC)_w}{A\tau} ln\left[\frac{1 - \frac{1}{F_1}\left(\frac{T_{w1}-T_a}{H}\right)}{1 - \frac{1}{F_1}\left(\frac{T_{w2}-T_a}{H}\right)}\right], \tag{29}$$

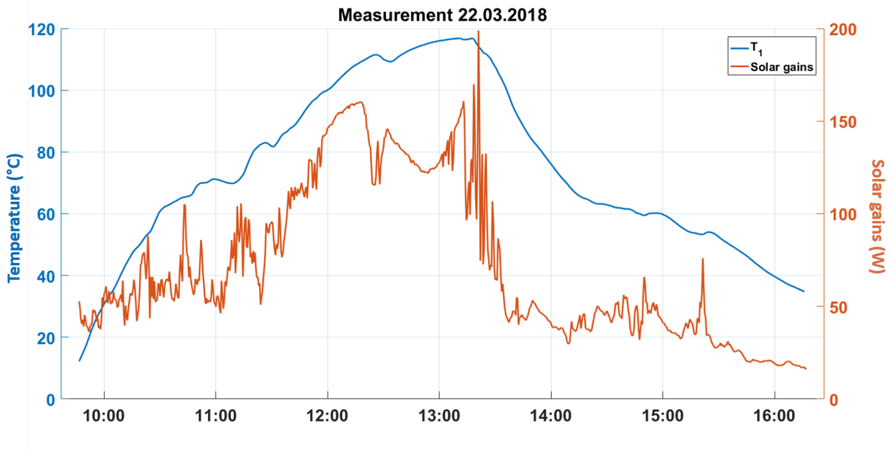

Figure 6: Temperature measurement - Empty pot - 22.03.2018

where F' is heat exchange efficiency factor, η_0 is optical efficiency, C_R is heat capacity ratio, M is the mass of water in kg, C is the heat capacity of water J kg^{-1} K^{-1}, A is aperture area, τ is time interval in seconds, T_{w1} is initial temperature of water, T_{w2} is final temperature of water, T_a is average ambient air temperature and H is the average solar radiation on horizontal surfaces in W m^{-2}.

And P_s using Eq. 30:

$$P_s = \frac{\Delta T(MC)_w}{\Delta t}, \tag{30}$$

where ΔT is a difference of temperature of 50°C and Δt the time needed to obtained it in seconds.

3. Results

Results of two temperature measurements on the lab roof are presented in Fig. 6 and 7. Temperatures up to 120°C are reached as early as March and show the good performance of ULOG despite its simple construction and raw materials. Solar gains are quite volatile. The temperature of the cooking pot follows the variations with a certain capacitance which smoothes the curve and delays it by just a few minutes. A time lag can indeed be observed in Fig. 6 between the large variations in the solar gains and T_1. This time lag is related to the time constant of the solar oven system. The effect of adding inertia due to the water is evident in Fig. 7. The blue curve is indeed much smoother than when the cooking vessel is empty. Moreover, the temperature stagnates when it reaches a few degrees above 100°C, caused by the water evaporation phenomenon.

From Fig. 6, the first figure of merit F_1, which is determined using Eq. 28, can be calculated. It is found to be 0.15 m^2 °C W^{-1} (taking into account an average solar irradiation of 660 W, an exterior temperature of 15°C and a maximum temperature of 116°C). From Fig. 7 and using Eq. 29, F_2 was calculated to be 0.315 . From the same set of data, a cooking power P_s=30.9 W was determined according to the Funk procedure, Eq. 30 with a difference of temperature of 50°C (between 40°C and 90°C), which was reached after 1h53min.

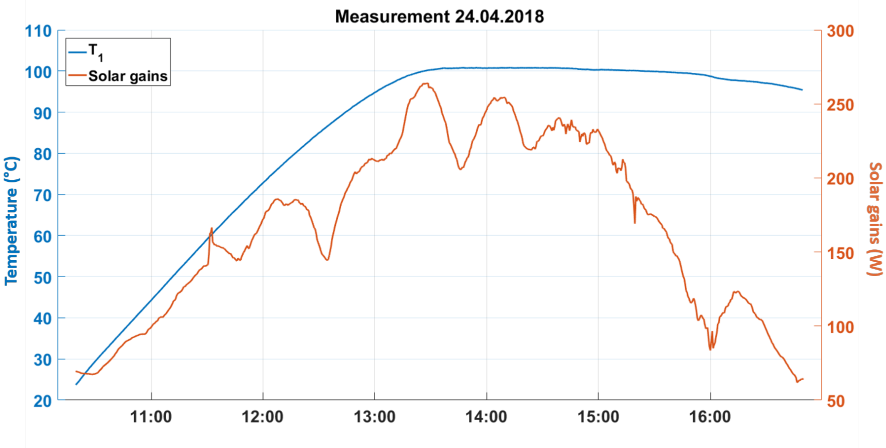

Figure 7: Temperature measurement - Pot with 1L of water - 24^{th} April 2018

Table 3: U-values through the five walls of the solar oven

West wall	Back wall	East wall	Front wall	Bottom wall
0.31	0.33	0.39	0.38	0.35

3.1. Model parameters

In this section, thanks to the experiments and measurements detailed previously, the value of the parameters G_{ij} and C_i are determined. It represents a first estimate of their value through analytical and experimental procedures and serves as nominal value for the sensitivity and optimization steps.

3.1.1. Conductances

The average of the five measurements of the U-value on the different surfaces of the oven are presented in Table 3. The U-values are given in $\left[\frac{W}{m^2K}\right]$. The differences in the values are mainly due to heterogeneity of the insulating wool and the wooden structure being slightly different in the five walls. The wool thickness and density are indeed quite different depending on the surface. The heat transfer coefficient of the wall U_{wall} of the solar oven is calculated as the average of the value of the five walls. It yields $U_{wall} = 0.35\left[\frac{W}{m^2K}\right]$. G_{23} is equal to U_{wall} times the walls area A_{wall} which is taken as the mean between the inner and the outer surface areas. Therefore $G_{23} = 0.19\left[\frac{W}{K}\right]$.

In a similar way that for G_{23}, an overall heat transfer coefficient for the window U_{glass} of $3\left[\frac{W}{m^2K}\right]$ can be determined. With the area of the window equal to 0.2025 $[m^2]$, it gives for the conductance $G_{56} = 0.61\left[\frac{W}{K}\right]$.

G_{46} and G_{24} represent the heat losses due to the thermal bridges of the oven. They are difficult to measure but they can be deduced from the U-value experiment. The heat balance at steady-state is written as

$$\dot{Q}_{heater} = U_{wall}A_{wall}\Delta T + U_{glass}A_{glass}\Delta T + \left(\psi_{frame}L_{frame} + \psi_{oven}L_{oven}\right)\Delta T \qquad (31)$$

The heat supplied by the heaters $\dot{Q}_{heater}$ equals the heat losses through the walls, the window and the thermal bridges of the window frame and the oven. ψ_{frame} and ψ_{oven} are the linear thermal transmittances of the thermal bridges and L_{frame} and L_{oven} are the length of the thermal bridges. $\dot{Q}_{heater}$ can be written as function of the global heat transfer coefficient of the oven to get

$$U_{tot}A_{tot} = U_{wall}A_{wall} + U_{glass}A_{glass} + \psi_{frame}L_{frame} + \psi_{oven}L_{oven} \tag{32}$$

By recognizing that $\psi_{frame}L_{frame}$ and $\psi_{oven}L_{oven}$ are respectively equal to G_{46} and G_{24}, since the other terms of Equation 32 are known, the following result is available

$$G_{24} + G_{46} = 0.03 \left[\frac{W}{K}\right] \tag{33}$$

As a first assumption, the thermal losses due to the thermal bridges are equally distributed among G_{24} and G_{46}. Thus, they are both equal to $0.015 \left[\frac{W}{K}\right]$. These heat losses due the thermal bridges represent slightly more than 5% of the total heat losses through the envelope.

The infiltration rate is found to be equal to $0.5 \left[\frac{vol}{h}\right]$. Knowing the infiltration rate λ, the air leakage mass flow is simply given by

$$\dot{m}_{leak} = \frac{\lambda \rho_{air} V_{oven}}{3600} = 4.63 \cdot 10^{-6} \left[\frac{kg}{s}\right] \tag{34}$$

where ρ_{air} is the air density and V_{oven} is the air volume inside the oven. The air properties are given in the appendices and the oven volume is equal to 0.031 $[m^3]$. The conductance G_{47} is therefore evaluated as the quantity

$$G_{47} = \dot{m}_{leak}c_{p,air} = 0.005 \left[\frac{W}{K}\right], \tag{35}$$

with $c_{p,air}$ being the specific heat capacity of air. It can be noted here that the heat losses due to air leakage are assumed to be very small and as such are do not play an important role in the heat balance.

It is assumed that the heat transfer between the node 1 and 2 is largely dominated by the conduction through the bottom of the cooking pot compared to the radiative heat transfer. The conduction through the bottom of the cooking vessel $A_{cv,bot}$ is evaluated with the following formula

$$G_{12} = A_1 \frac{1}{\frac{\Delta_1}{k_1 A_{cv,bot}} + \frac{1}{h_c A_{cv,bot}} + \frac{\Delta_2}{k_2 A_{cv,bot}}} \tag{36}$$

The thermal resistance due to the interface between the pot and the inner wall is taken into account with the thermal contact conductance coefficient h_c fixed to $10 \left[\frac{W}{m^2K}\right]$ from Fletcher (1972). Δ_1 and Δ_2 are the thickness of the nodes 1 and 2 and are fixed to 0.5 $[cm]$ and 15 $[cm]$. It yields $G_{12} = 0.36 \left[\frac{W}{K}\right]$

3.1.2. Capacitances

The cooking vessel is made of iron. The specific heat capacity of iron taken from the literature is presented in the appendices and a balance is used to know the mass. The result is $C_1 = 456 \left[\frac{J}{K}\right]$. When the cooking vessel is filled with 1L of water, it corresponds to an addition of $4140 \left[\frac{J}{K}\right]$.

Due to the heterogeneous structure of the oven's walls, it is not straightforward to determine their capacitances. The walls are made of a thin aluminium foil on the inner side, a wood structure filled with wool and a thin wood panel at the exterior. The mass of every component is estimated for a particular wall. Their masses are then multiplied by their specific heat capacity and the sum of these results corresponds to the capacitance of the particular wall. The same procedure is applied for each wall and the sum represents the global wall capacitance of the oven.

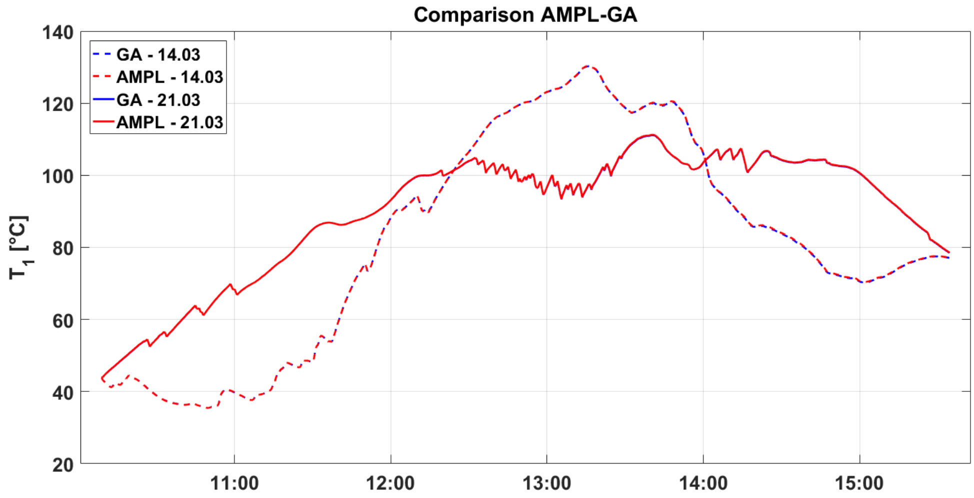

Figure 8: Results of optimization for Genetic Algorithm and AMPL

The aluminium foil and half of the inside structure are allocated to the inner wall node while the other half of the wood structure and the outer wood panel are allocated to the outer wall capacitance. The results are $C_2 = 2819$ and $C_3 = 4979 \left[\frac{J}{K}\right]$.

The capacitances of the glass layers have been estimated in previous work on the glazing done at the laboratory and correspond to $C_5 = C_6 = 1418 \left[\frac{J}{K}\right]$.

The capacitance of the inside air is evaluated by the multiplication of the volume of the oven, the air density ($1.08 \left[\frac{kg}{m^{-3}}\right]$) and specific heat ($1008.7 \left[\frac{J}{kgK}\right]$). It yields $C_7 = 34 \left[\frac{J}{K}\right]$. The ratio of solar gains allocated to the cooking pot and the inner wall is determined through the resolution of the integral. It gives a value for R_{Surf} very close to 0.2.

3.2. Optimization

In order to have confidence in the optimization results, the first test done is the comparison between the two methods: GA and AMPL. Large and similar bounds are set to the variables for both GA and AMPL procedures with the same objective function. The results of the optimization for two different days are presented in Fig. 8. The similarities between the two approaches are high. For the majority of the conductances and capacitances, the two methods present different values but for the most important parameters (identified by a sensitivity analysis not shown here), the values are similar between the two approaches. This explains the almost identical curves in Fig. 8 and gives confidence in the methods. The GA procedure is preferred for the rest of the study for its simple implementation in Matlab.

The optimization procedure has finally been implemented with the objective function defined by Equation 23. The results for the five sets of measurements are presented in Figs. 9-13.

The mean relative errors between the measured and simulated cooking vessel temperature for the five measurements are shown in the following Table 4. The simulation is in good agreement with the measurements, with errors either below or around 7%. Especially for the sets from 11^{th} April and 19^{th} April with low relative errors. The fluctuations of T_1 in Fig. 9 and 10 are well reproduced by the simulated temperature. However, for the 19^{th}, 24^{th} and 26^{th} April measurements, the heating process is not perfectly reproduced by the optimization. The curvatures of

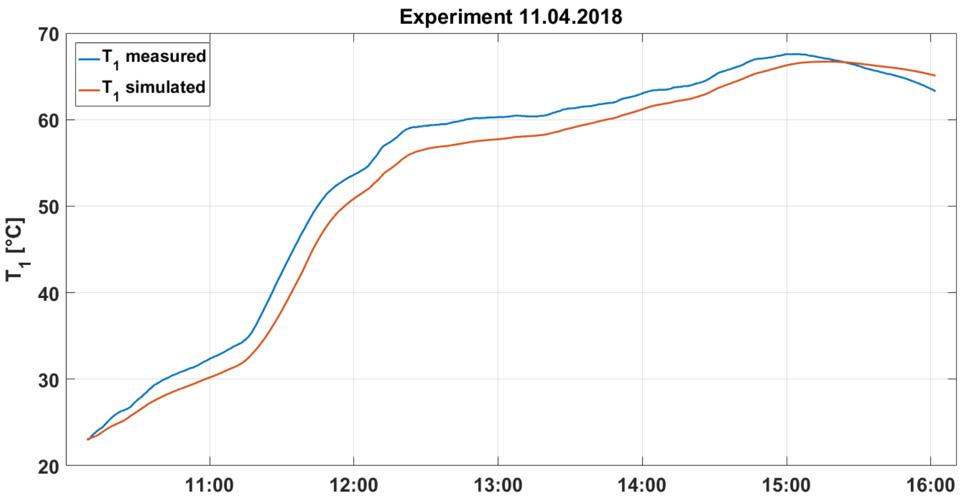

Figure 9: Results of optimization - 11^{th} April 2018

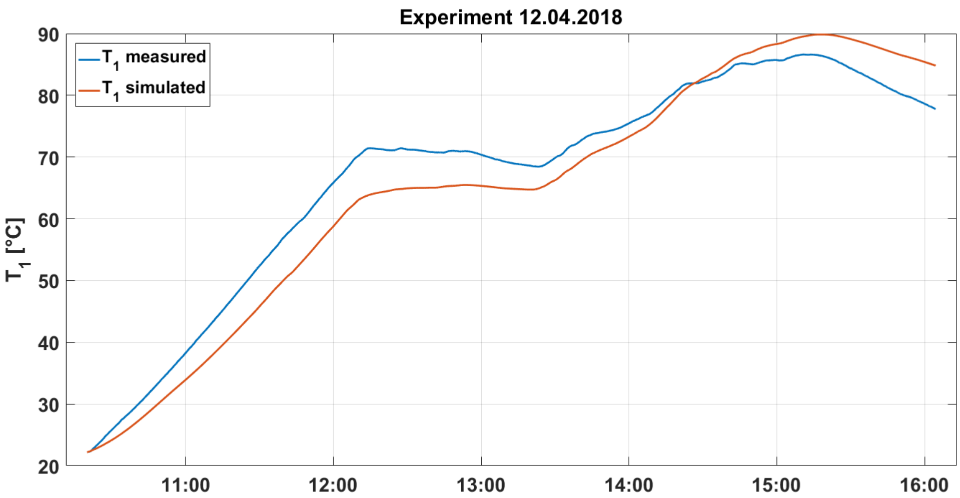

Figure 10: Results of optimization - 12^{th} April 2018

Table 4: Relative error on T_1 for the five experiments conducted in April 2018

Measurement	11^{th}	12^{th}	19^{th}	24^{th}	26^{th}
Relative error [%]	4.08	6.81	3.81	5.52	7.22

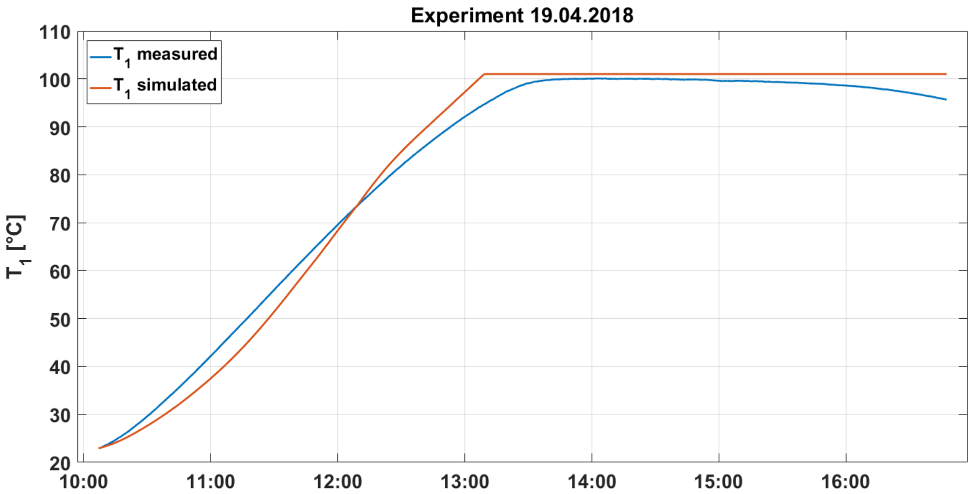

Figure 11: Results of optimization - 19^{th} April 2018

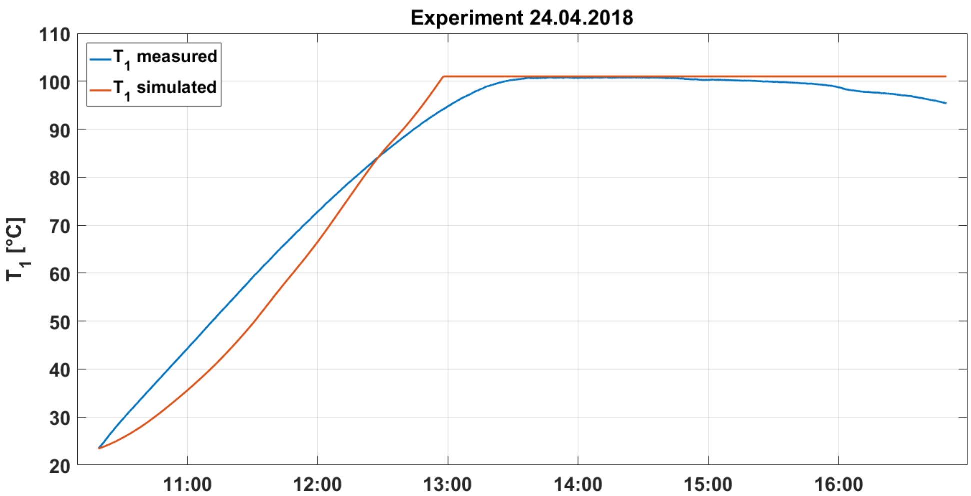

Figure 12: Results of optimization - 24^{th} April 2018

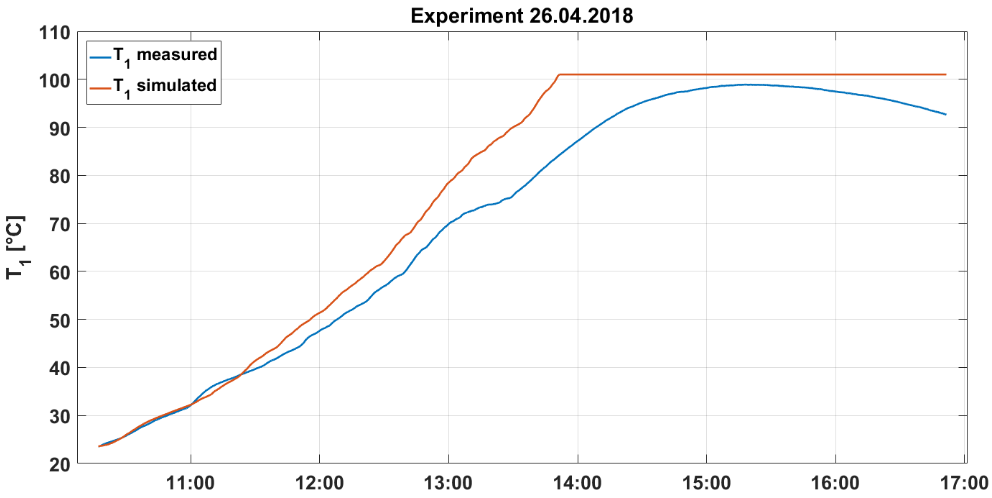

Figure 13: Results of optimization - 26^{th} April 2018

Conductances, $\left[\frac{W}{K}\right]$		Capacitances, $\left[\frac{J}{K}\right]$	
G_{12}	2.38	C_1	5974.8
G_{16}	11.11	C_2	2792.4
G_{23}	0.32	C_6	1843.4
G_{45}	1.13		
G_{56}	1.22		

Table 5: Optimized parameters values

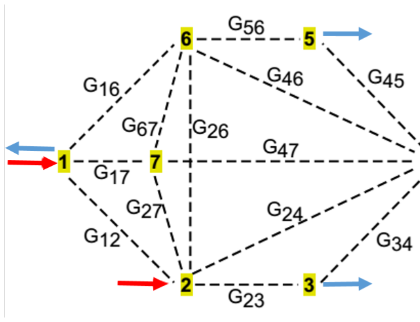

Figure 14: Schematic representation of the nodal network, conductances and energy inputs (arrows)

the two curves are quite different. This is obvious in Fig. 13 where the simulated curve heats up too quickly.

Based on the results from the optimization, the parameter values given in Table 5 are used in the model.

The worst fit occurs for the data set from the 26^{th} April. It may indicate the presence of errors in these measurements. The optimization is thus tried without this set of data given to the objective function. Slightly better results are then obtained, especially for the 11.04 and 12.04 experiments shown in Figs. 15 and 16. As can be seen in Table 6, the error is almost divided by two for the first measurement. The others are also slightly smaller than in the scenario with the five measurements given to the objective function. It is interesting to note that the optimized values of the parameters are similar to the previous scenario except C_2 whose optimized value decreases to $2119.6\left[\frac{J}{K}\right]$.

All the simulated temperatures of the oven nodes are presented in Fig. 17. While the main focus was on T_1, it is also interesting to analyse the other results of the model simulation. As expected, the temperatures of the nodes connected with the environment T_3 and T_5 are close

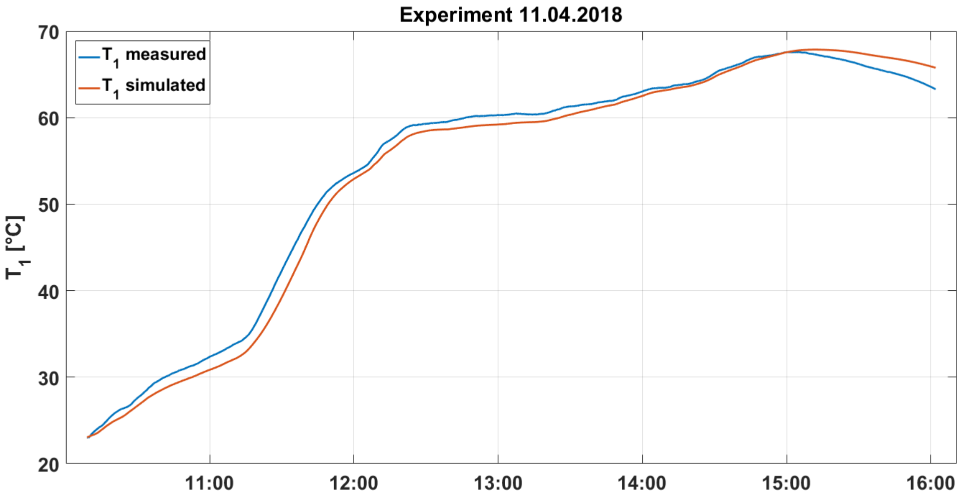

Figure 15: Results of optimization - 11^{th} April 2018

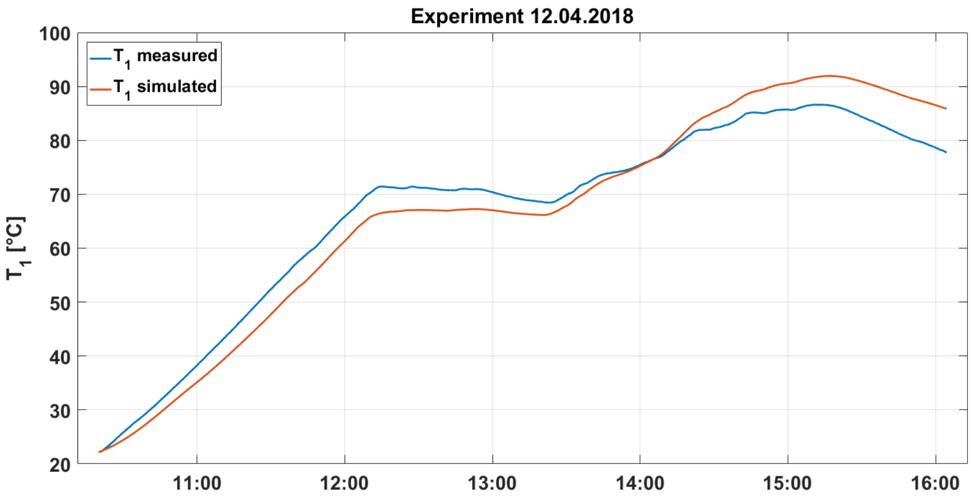

Figure 16: Results of optimization - 12^{th} April 2018

Table 6: Relative error on T_1 for the five experiments conducted in April 2018

Measurement	11^{th}	12^{th}	19^{th}	24^{th}	26^{th}
Relative error [%]	2.26	5.61	3.72	4.98	8.89

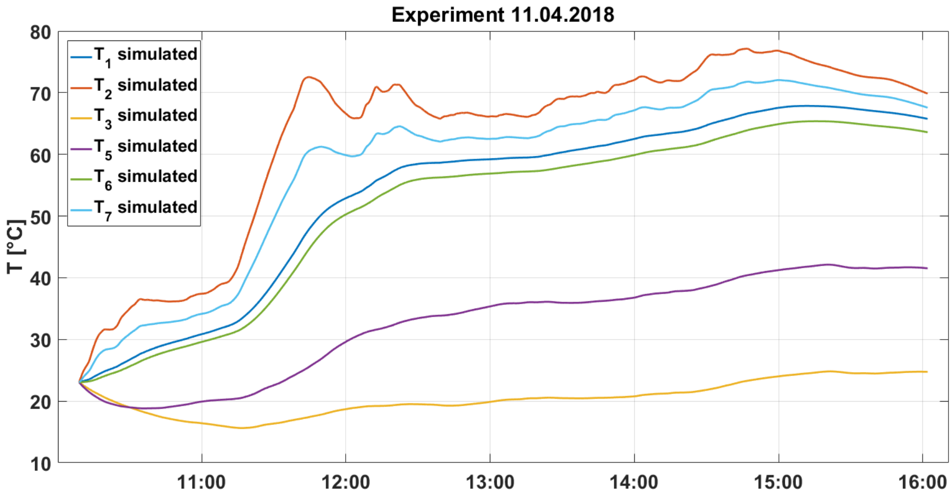

Figure 17: All simulated nodes temperatures for the data set of 11^{th} April 2018

to the ambient temperature. The slightly higher temperature T_5 indicates the higher thermal losses through the glass layer. T_2 and T_7 correspond to nodes with relatively low capacitances and are therefore more volatile. Due to the high conductance between the nodes 5 and 6, their temperatures are closely related. Even though the optimization only considered T_1, it increases the confidence into the validity of the model to see the others nodes' temperature values are also in an acceptable range and keeping their physical meaning.

The model is solved once by using the correlations for convective and radiative heat exchanges given in Sect. 2.4. The heat transfer coefficients are plotted in Fig. 18. h_{56} *rad.* is evaluated by the formula 20 and h_{56} *conv.* by Equation 16. Heat transfer coefficients with the ambient air are quite volatile due to the varying ambient temperature. Their values around 2.5 $\left[\frac{W}{m^2K}\right]$ are typical of processes involving natural convection. The relative high value for h_{56} *rad.* in comparison to h_{56} *conv.* indicates the importance of radiation processes between the two glass layers. The heat transfer coefficients for the confined air present also typical values for such convection processes.

Tests have been made with data set without water load in the cooking vessel. Due to the high volatility of the solar gains and the relatively large time step compared to these variations, the fit tends to be more difficult. An example of such results is shown in Fig. 19. The relative error is also quite low and the red curve follows the general trend of the blue curve. The simulated temperature however oscillates too much and reaches too high temperatures. The heat losses due the thermal bridges represent slightly more than 5% of the total heat losses through the envelope. The heat losses due to air leakage are very small and do not play an important role in the heat balance.

3.3. Potato days

The results of the cooking experiments are presented in Fig. 20 with the fitted curve. The alignment of the points in the $\frac{1}{T}$ against $\ln t_c$ plot shows a very good agreement with the Arrhenius theory. From these results, the following values for the activation energy ϕ, the pre exponential constant B and the cooking criterion CC are found.

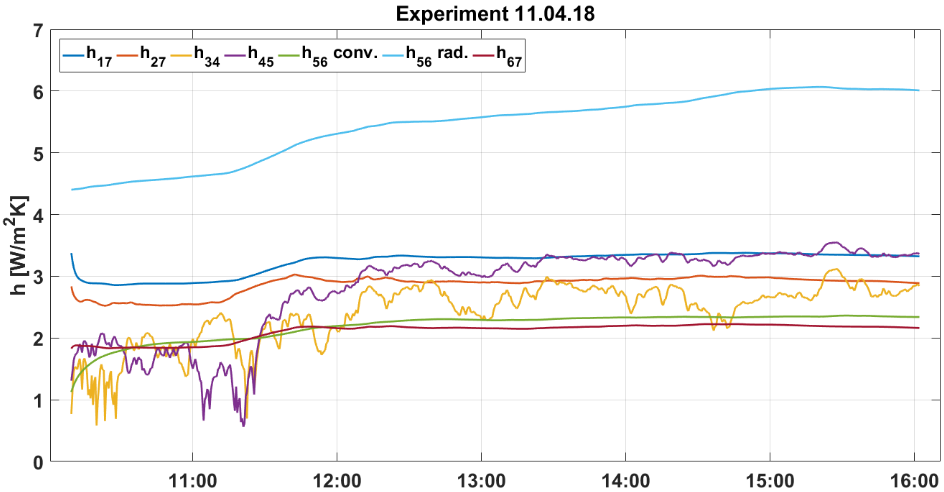

Figure 18: Heat transfer coefficients

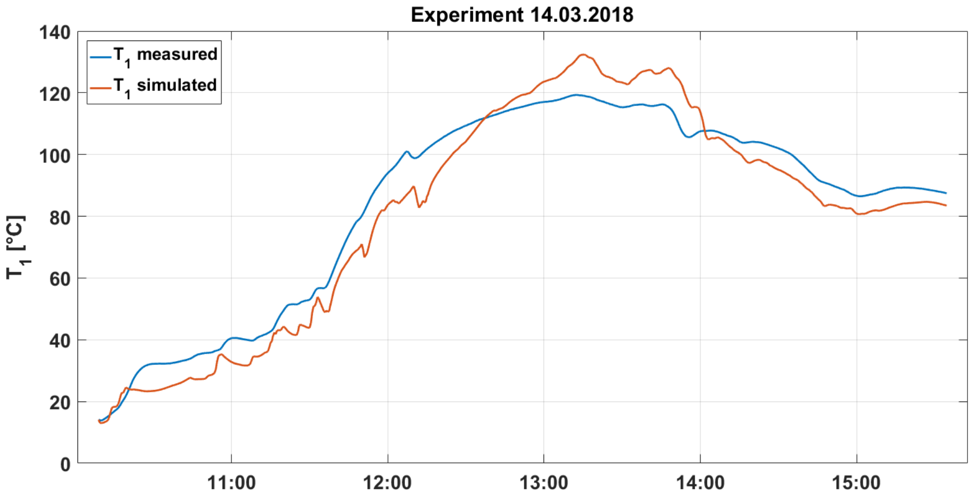

Figure 19: Results of optimization - 14.03.2018

Table 7: Results of the cooking experiments

Activation energy, $\left[\frac{kJ}{mol}\right]$	74.14
Pre-exponential factor, [s]	$9.93 \cdot 10^{14}$
Cooking criterion, [−]	$8.08 \cdot 10^{7}$

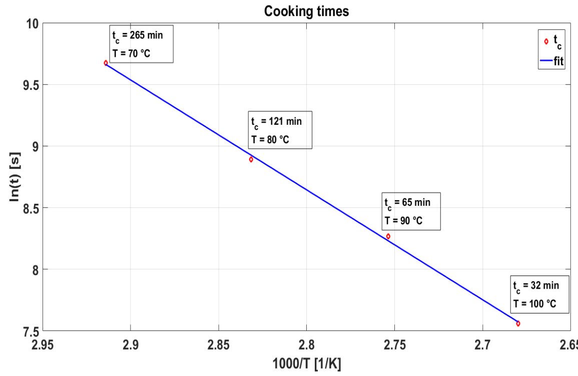

Figure 20: Cooking times versus cooking temperature

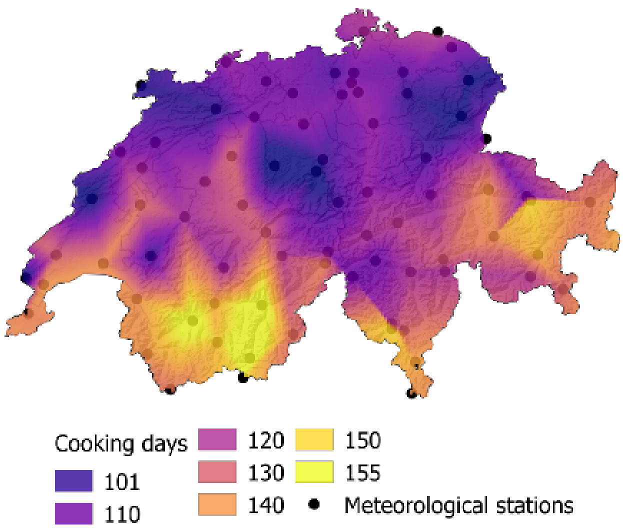

Figure 21: Results of simulation for a year without reflector

The threshold temperature under which it is assumed the potatoes would never cook is fixed to 60 °C. Indeed, for this temperature, the cooking time estimated with the fitted curve in Fig. 20 is longer than 9h. It could theoretically correspond to starting cooking in the morning and having the food ready in the evening. However, in practice this is not very likely to happen. As a higher cooking time is not acceptable, the threshold temperature of 60 °C is chosen. It also corresponds to the temperature above which the gelatinization of potato starch starts (Shiotsubo, 1984).

The "potato days" are calculated for the different meteorological stations in Switzerland. The results are then integrated in a map with QGIS and interpolated to obtain values for the whole Swiss territory. The triangular interpolation (TIN) method of QGIS is used. The results are presented in the following map. This map gives a first approximation of the possible use of a solar oven in Switzerland. The yellow areas represent the high potential. A maximum of more than 160 "potato days" is reached in Zermatt at 1640 $[m]$ in the South-East of the Canton of Valais. Cities, especially in French speaking Switzerland, offer also a significant potential. By contrast, the North of the territory is less favourable to solar cooking due to the smaller amount

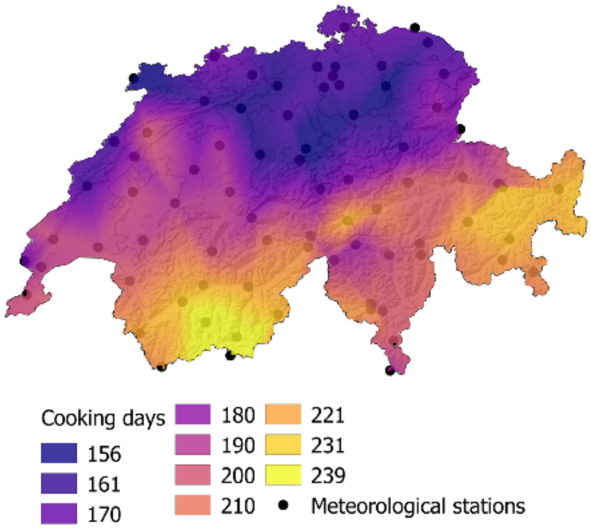

Figure 22: Results of simulation for a year with reflector

of solar irradiation.

The same procedure is applied to obtain the results with the reflector. They are shown in Fig. 22. A significant increase of the potential can be observed. A maximum of more than 240 "potato days" is reached at Pian Rosa at 3500 m height on the South-Eastern border of the Valais.

4. Discussion

The figures of merit for the ULOG solar oven were computed. Based on previous studies, F_1 should be in the range 0.12–0.16 m^2 °C W^{-1} whereas F2 should be in the range of 0.254–0.490. Therefore, the obtained values are within the recommended range (Yettou et al., 2014; Saxena et al., 2011) and compare well with other solar cookers (Harmim et al., 2012; Guidara et al., 2017).

The optimization algorithm tends to increase the capacitance of the cooking vessel-water and the glazing nodes. By contrast, the value for the inner wall capacitance is lower than its nominal value. This could indicate that the part of the inner wall that plays a role in the thermal inertia is less than half of the wall and that the important mass for heat exchanges is represented by the very first layers of the wall structure. The conductance between the cooking pot and the inner wall is considerably larger than the estimated nominal value. The radiative component that has been neglected in the first approximation could be responsible for this higher value of the conductance.

The conductance between the pot and the inner glass layer is significantly larger than the other conductances. It represents the radiative exchanges and such a high value probably overestimates the contribution of radiative phenomena. This highlights one of the drawbacks of an optimization process: the loss of physical meaning of the parameters. Due mainly to modelling errors, the optimization procedure finds the best value for the parameter to minimize the objective function, which can greatly diverge from the physical reality. The optimized U-value however is in good agreement with the experimental one.

The model seems to be in good accordance with the experimental data in particular as compared to the maximum temperature obtained. This is comparable to results from Zafar et al. (2019) and the error range between the simulated and measured values are also in line with previous studies (Guidara et al., 2017). The focus has mainly been on the results with a water load, which represents the principal situation in which the oven will be practically used. This model with high capacitance is optimized more easily than sensitive models. It tends to smooth the results and attenuate the effects of solar irradiation variations. These variations are low during a sunny day without clouds. During such days, the solar gains follow a smooth curve which facilitates the optimization process. On cloudy days, the solar irradiation can drastically change in an instant. A large amount of this information is lost due to the time step of 30 seconds which is much larger than the phenomena involved in the solar irradiation fluctuations. Tests have been performed with smaller time steps in order to capture these sharp variations. However, the data set and the computing time become very large and the fitting is quite difficult.

It can also be noted in Figs. 9-12 that there appears to be a shared feature in the computation of the temperature. A slightly lower temperature is simulated in the first hours of the day while the contrary (higher temperatures simulated) are obtained in the last hours of the day. It is possible that this could be due to the use of an infiltration rate that was not temperature dependent. Similar findings have also been reported by Koinakis (2005). A fixed infiltration rate means that the model did not account, for example, for the varying pressure inside the box Han et al. (2015).

The very good fit of the potato cooking times in Fig. 20 demonstrates that the cooking process is well described by an Arrhenius law. The cooking times of potatoes double when the cooking temperature decreases by 10 $°C$. In Shiotsubo (1984), an activation energy for the starch gelatinization of around $99 \pm 25 \left[\frac{kJ}{mol}\right]$ is presented. The value found in the present study is slightly lower but still in good agreement with the literature. The difference could be explained by the fact that the whole potatoes cooking process is characterized in this study while only the starch gelatinization reaction is considered in (Shiotsubo, 1984). This chemical reaction may be dominant but it is not the only chemical process involved in cooking.

The results of the simulation over a year show the good potential for solar oven utilization in Switzerland. It is indeed possible to cook potatoes more often than every other day. The calculation of the reflector contributions to the solar gains is very simplified since it takes into account a fixed and optimal value for its apparent surface. Hence this method overestimates the reflector contributions. However, it gives useful information on the order of magnitude of the performance enhancement due to the reflector. The effects of the reflector remains however significant since it increases the number of "potato days" by around 50%. It is known that the South of Switzerland receives more solar radiation and is thus more propitious for solar cooking. Good performances were thus observed at high altitude and encourages the solar cooking utilization in isolated locations such as a mountain refuge hut. A comparative analysis of the meteorological data from Jungfraujoch (located at 3580 m) and from Pully (located at 461 m), revealed that although the air temperature was on average 18 K lower at higher altitudes, the incoming solar irradiation was on average 31% higher at the Jungfraujoch (with above 60% more irradiation in December and January). This highlights the fact that more than the ambient temperature, the amount of solar radiation is the main parameter for solar cooking. Cities with ambient temperatures slightly higher than their surrounding countryside are also favourable to solar cooking, assuming a good solar exposure. The interpolation in the GIS induces some unrealistic results. Such anomaly can be observed at the far East of the Switzerland, in the Grisons or around Bern with the presence of a cross. They are characterized by sharp colour variation on a straight line, which represents obviously not the physical reality but only results of interpolating numerical processes. In reality, such a sharp colour variation could be caused by shadowing effects due to the land surface and relief. Mountains or valleys for instance could cause local solar irradiation variations and lead to a decrease of "potato days". This would however necessitate real irradiation data for the whole Swiss territory which is quasi impossible to obtain. The interpolation is useful to get an approximation of such data but its results must be interpreted with care.

5. Conclusions

This study has presented an innovative nodal model for the Swiss ULOG solar oven, which predicts the cooking vessel temperature's profile along the day with solar irradiation and ambient temperature as inputs.

The model parameters, depending on the physical properties of the oven, are determined analytically when correlations are available, experimentally or through an optimization procedure. Overall, the model is able to predict the pot temperature with average relative errors around 5%. In an upcoming study, the model will be improved by using an adaptive infiltration rate which will be based on the formulations proposed by Malik (1978); Han et al. (2015) and by incorporating new measured data that will be collected for the solar cooker.

Based on these reliable results and thanks to the new metric developed, the model is used to assess the solar cooking potential over the Swiss territory. The North-East of Switzerland is the least favourable region for solar cooking, with theoretically around 155 cooking days per year. On the other hand, almost 240 cooking days are reached in the Valais and the Grisons. Similar results are obtained even for locations at high altitude. This is an encouraging conclusion, which supports the initial assumption that solar cooking is suitable for remote places such as high altitude areas. The study highlights a significant potential for solar cooking in Switzerland.

Nowadays, solar cooking is still anecdotal in Switzerland and the potential is far from being fully exploited. Obviously, solar cooking will not completely replace standard cooking, due to its long cooking times, the good solar exposure needed and habits. However solar cooking interest is likely to increase and the corresponding awareness might contribute to reducing the high energy consumption per household in Switzerland.

Acknowledgements

The authors would like to thank the ENAC Innoseed program for its financial support for this project. This research project has been financially supported by the Swiss Innovation Agency Innosuisse through the Swiss Competence Center for Energy Research SCCER FEEB&D. The authors would also like to acknowledge the work performed by Alexandre Diévart in the conception of the new solar cooker.

Nomenclature

ΔT	Temperature difference between the air inside and outside of the oven, [K]
Δ	Thickness of the node, $[m]$
$\dot{m}_{leak}$	Air leakage mass flow, $[\frac{\mathrm{kg}}{\mathrm{s}}]$
$\dot{m}_{leak}$	Air leakage mass flow, $[\frac{kg}{s}]$
$\dot{Q}$	Heat transfer rate, [W]

$\dot{q}$ Heat flux, $\left[\frac{W}{m^2}\right]$

$\dot{Q}_{heater}$ Heat supply of the heaters, [W]

ϵ Emissivity, $[-]$

γ Solar incident angle, $[°]$

ϕ Activation energy, $\left[\frac{kJ}{mol}\right]$

ψ_{frame} Linear thermal transmittance of the frame thermal bridge, $[\frac{W}{mK}]$

ψ_{frame} Linear thermal transmittance of the frame thermal bridge, $[\frac{\mathrm{W}}{\mathrm{mK}}]$

ψ_{oven} Linear thermal transmittance of the oven thermal bridge, $[\frac{W}{mK}]$

ψ_{oven} Linear thermal transmittance of the oven thermal bridge, $[\frac{\mathrm{W}}{\mathrm{mK}}]$

ρ Density, $\left[\frac{\mathrm{kg}}{\mathrm{m}^3}\right]$

ρ Density, $\left[\frac{kg}{m^3}\right]$

σ Stefan-Boltzmann constant, $\left[\frac{W}{m^2K^4}\right]$

A Surface area, $[m^2]$

A_{bd} Albedo coefficient, $[-]$

$A_{cv,bot}$ Bottom surface area of the cooking vessel, $[m^2]$

$A_{cv,lid}$ Surface area of the cooking vessel lid, $[m^2]$

$A_{cv,v}$ Surface area of the lateral walls of the cooking vessel, $[m^2]$

A_{cv} Total surface area of the cooking vessel, $[m^2]$

A_{glass} Surface area of the glass, $[m^2]$

A^*_{glass} Apparent surface area of the glass, $[m^2]$

A_{refl} Surface area of the reflectors, $[m^2]$

A^*_{refl} Apparent surface area of the reflectors, $[m^2]$

A_{tot} Surface area of the oven's envelope, $[\mathrm{m}^2]$

A_{wall} Surface area of the oven walls, $[m^2]$

B Pre-exponential factor

C_i Capacitance, $[\frac{\mathrm{J}}{\mathrm{K}}]$

c_p Specific heat capacity, $[\frac{\mathrm{J}}{\mathrm{kgK}}]$

$E_{b,i}$ Black body emissive power, $\left[\frac{W}{m^2}\right]$

F_1 First figure of merit, m^2 °C W^{-1}

F_2 Second figure of merit, m^2 °C W^{-1}

F_{ij} View factor, $[-]$

G Solar gains, [W]

g Solar heat gain coefficient, $[-]$

g_{dif} Diffuse solar heat gain coefficient, $[-]$

g_{dir} Direct solar heat gain coefficient, $[-]$

G_{ij} Conductance, $[\frac{\mathrm{W}}{\mathrm{K}}]$

h Convective heat transfer coefficient, $[\frac{W}{m^2K}]$

h_c Thermal contact conductance coefficient, $\left[\frac{W}{m^2K}\right]$

$h_{cv,lid}$ Heat transfer coefficient between the air and the lid, $\left[\frac{W}{m^2K}\right]$

$h_{cv,v}$ Heat transfer coefficient between the air and the lateral walls of the cooking vessel, $\left[\frac{W}{m^2K}\right]$

i_{diff} Diffuse solar irradiation, $[\frac{W}{m^2}]$

i_{dir} Direct solar irradiation, $[\frac{W}{m^2}]$

k Thermal conductivity, $[\frac{W}{mK}]$

L Length, $[m]$

L_{frame} Length of the window frame thermal bridge, $[m]$

L_{frame} Length of the window frame thermal bridge, [m]

L_{oven} Length of the oven thermal bridge, $[m]$

L_{oven} Length of the oven thermal bridge, [m]

m Mass, [kg]

Nu Nusselt number, $[-]$

P Cooking power, W

Pr Prandtl number, $[-]$

R Universal gas constant, $\left[\frac{J}{molK}\right]$

r Rate constant

R_{ij} Resistance, $[\frac{\mathrm{K}}{\mathrm{W}}]$

Ra Rayleigh number, $[-]$

T Temperature, [K]

t_0 Starting time of cooking period, $[s]$

t_c Cooking time, $[s]$

$T_{1,Mes}$ Measured cooking vessel temperature, $[K]$

$T_{2,Mes}$ Measured inner wall temperature, $[K]$

t_{end} Ending time of the cooking period, $[s]$

U Overall heat transfer coefficient, $[\frac{\mathrm{W}}{\mathrm{m^2K}}]$

U_{glass} Overall heat transfer coefficient of the oven window, $[\frac{W}{m^2K}]$

U_{wall} Overall heat transfer coefficient of the oven walls, $[\frac{W}{m^2K}]$

V_{oven} Volume inside the oven, $[\mathrm{m}^3]$

V_{oven} Volume inside the oven, $[m^3]$

References

Al-Soud, M. S., Abdallah, E., Akayleh, A., Abdallah, S., Hrayshat, E. S., 2010. A parabolic solar cooker with automatic two axes sun tracking system. Applied Energy 87, 463–470.

Associates, K., 2000. Thermal Network Modeling Handbook. K&K Associates.

Baehr, H. D., Stephan, K., 2011. Heat and Mass Transfer, 3rd Edition. Springer.

Banos, R., Manzano-Agugliaro, F., Montoya, F. G., Gil, C., Alcayde, A., Gómez, J., 2011. Optimization methods applied to renewable and sustainable energy: A review. Renewable and Sustainable Energy Reviews 15, 1753:1766.

Association Solemyo, 2019.
URL http://www.cuisinesolaire.com/solemyo/Accueil/

Solar Topo, 2019. Sun position Calculator.
URL http://www.solartopo.com/solar-orbit.htm

Blahovec, J., Esmir, A. A. S., Vacek, J., 2000. Objective method for determination of potato cooking. Agricultural Engineering International: the CIGR Journal of Scientific Research and Development 2.

Churchill, S. W., Chu, H. H. S., 1975. Correlating equations for laminar and turbulent free convection from a vertical plate. International Journal of Heat and Mass Transfer 18, 1323:1329.

de Saussure, H. B., 1784. Héliomètre.
URL https://fr.wikipedia.org/wiki/Horace_B%C3%A9n%C3%A9dict_de_Saussure#H%C3%A9liothermom%C3%A8tre_:_l'anc%C3%AAtre_du_capteur_solaire_(1774

Esen, M., 2004. Thermal performance of a solar cooker integrated vacuum-tube collector with heat pipes containing different refrigerants 76 (6), 751–757.
URL http://www.sciencedirect.com/science/article/pii/S0038092X04000027

Fletcher, L. S., 1972. A review of thermal control materials for metallic jonctions. Journal of Spacecraft and Rockets 12, 849:850.

Fourer, R., Gay, D. M., Kernighan, B. W., 2003. AMPL: A Modeling Language for Mathematical Programming, 2nd Edition. Duxbury Thomson.

Funk, P. A., 2000. Evaluating the international standard procedure for testing solar cookers and reporting performance 68 (1), 1–7.
URL http://www.sciencedirect.com/science/article/pii/S0038092X99000596

Geddam, S., Dinesh, G. K., Sivasankar, T., 2015. Determination of thermal performance of a box type solar cooker. Solar Energy 113, 324:331.

Gnansounou, E., 2014. Energétique du bâtiment.

Guidara, Z., Souissi, M., Morgenstern, A., Maalej, A., 2017. Thermal performance of a solar box cooker with outer reflectors: Numerical study and experimental investigation. Solar Energy 158, 347–359.

Han, G., Srebric, J., Enache-Pommer, E., Jan. 2015. Different modeling strategies of infiltration rates for an office building to improve accuracy of building energy simulations. Energy and Buildings 86, 288–295.
URL http://www.sciencedirect.com/science/article/pii/S0378778814008731

Harmim, A., Merzouk, M., Boukar, M., Amar, M., 2012. Performance study of a box-type solar cooker employing an asymmetric compound parabolic concentrator 47 (1), 471–480.
URL http://www.sciencedirect.com/science/article/pii/S0360544212007153

Incropera, F. P., Dewitt, D. P., Bergman, T. L., Lavine, A. S., 2013. Foundations of Heat Transfer, sixth Edition. John Wiley & Sons.

Koinakis, C. J., Apr. 2005. Combined thermal and natural ventilation modeling for long-term energy assessment: validation with experimental measurements. Energy and Buildings 37 (4), 311–323.
URL http://www.sciencedirect.com/science/article/pii/S0378778804002129

Löf, G. O. G., 1963. Recent investigations in the use of solar energy for cooking. Solar Energy 7, 125:133.

Malik, N., Apr. 1978. Field studies of dependence of air infiltration on outside temperature and wind. Energy and Buildings 1 (3), 281–292.
URL http://www.sciencedirect.com/science/article/pii/0378778878900087

Mannan, S., 2005. Lee's Loss Prevention in the Process Industries: Hazard Identification, Assessment and Control, 3rd Edition. Vol. 1. Elsevier.

Modest, M. F., 2003. Radiative Heat Transfer, 2nd Edition. Academic Press.

Mullick, S. C., Kandpal, T. C., Saxena, A. K., 1987. Thermal test procedure for box-type solar cookers. Solar Energy 4, 353:360.

Olsommer, B., von Spakovsky, M., Favrat, D., 1997. Transfert de chaleur par rayonnement dans un four d'incinération industriel: application de la méthode des zones. Revue Générale de Thermique 36, 125–134.

Panwar, N. L., Kaushik, S. C., Kothari, S., 2012. State of the art of solar cooking: An overview 16 (6), 3776–3785.
URL http://www.sciencedirect.com/science/article/pii/S1364032112002092

Petrou, A. L., Roulia, M., Tampouris, K., 2002. The use of the arrhenius equation in the study of deterioration and of cooking of foods - some scientific and pedagogic aspects. Chemistry Education: Research and Practice in Europe 3, 87:97.

Remund, J., 2008. Quality of meteonorm version 6.0 6 (1), 389.
URL http://www.meteotest.ch/fileadmin/user_upload/Sonnenenergie/pdf/2008WREC_mn6_qual_paper.pdf

Remund, J., Müller, S. C., Schilter, C., Rihm, B., 2010. The use of meteonorm weather generator for climate change studies. In: 10th EMS Annual Meeting, 10th European Conference on Applications of Meteorology (ECAM) Abstracts, held Sept. 13-17, 2010 in Zürich, Switzerland. http://meetings. copernicus. org/ems2010/, id. EMS2010-417. Vol. 1. p. 417.
URL http://adsabs.harvard.edu/abs/2010ems..confE.417R

Saha, G., Saha, S., Islam, M. Q., Akhanda, M. A. R., 2007. Natural convection in enclosure with discrete isothermal heating from below. Journal of Naval Architecture and Marine Engineering 4, 1:13.

Saxena, A., Varun, Pandey, S., Srivastav, G., 2011. A thermodynamic review on solar box type cookers. Renewable and Sustainable Energy Reviews 15, 3301–3318.

Schüler, A., Geng, J., Oelhafen, P., Brunold, S., Gantenbein, P., Frei, U., 2000. Application of titanium containing amorphous hydrogenated carbon films (a-c:h/ti) as optical selective solar absorber coatings. Solar Energy Materials & Solar Cells 60, 295:307.

Schwarzer, K., da Silva, M. E. V., 2008. Characterisation and design methods of solar cookers. Solar Energy 82, 157:163.

Sethi, V. P., Pal, D. S., Sumanthy, K., 2014. Performance evaluation and solar radiation capture of optimally inclined box type solar cooker with parallelepiped cooking vessel design. Energy Conversion and Management 81, 231:241.

Shiotsubo, T., 1984. Gelatinization temperature of potato starch at the equilibrium state. Agricultural and Biological Chemistry 48, 1:7.

Soria-Verdugo, A., 2015. Experimental analysis and simulation of the performance of a box-type solar cooker. Energy for Sustainable Development 29, 65–71.

Terres, H., Lizardi, A., López, R., Vaca, M., Chávez, S., 2014. Mathematical model to study solar cookers box-type with internal reflectors. Energy Procedia 57, 1583–1592.

Yettou, F., Azoui, B., Malek, A., Gama, A., Panwar, N., 2014. Solar cooker realizations in actual use: An overview. Renewable and Sustainable Energy Reviews 37, 288–306.

Zafar, H. A., Badar, A. W., Butt, F. S., Khan, M. Y., Siddiqui, M. S., 2019. Numerical modeling and parametric study of an innovative solar oven 187, 411–426.
URL http://www.sciencedirect.com/science/article/pii/S0038092X19305468